The Journal of Experimental Biology 214, 2036-2046

doi:10.1242/jeb.047159

RESEARCH ARTICLE

Kinematics of the quadrate bone during feeding in mallard ducks

Megan M. Dawson[1,*], Keith A. Metzger[1,2], David B. Baier[1,3] and Elizabeth L. Brainerd[1]

[1]Department of Ecology and Evolutionary Biology, Brown University, Providence, RI 02912, USA, [2]Hofstra North Shore-LIJ School of Medicine at Hofstra University, Hempstead, NY 11549, USA and [3]Department of Biology, Providence College, Providence, RI 02912, USA

*Author for correspondence (Megan_Dawson@brown.edu)

Accepted 5 March 2011

SUMMARY

Avian cranial kinesis, in which mobility of the quadrate, pterygoid and palatine bones contribute to upper bill elevation, is believed to occur in all extant birds. The most widely accepted model for upper bill elevation is that the quadrate rotates rostrally and medially towards the pterygoid, transferring force to the mobile pterygoid–palatine complex, which pushes on the upper bill. Until now, however, it has not been possible to test this hypothesis *in vivo* because quadrate motions are rapid, three-dimensionally complex and not visible externally. Here we use a new *in vivo* X-ray motion analysis technique, X-ray reconstruction of moving morphology (XROMM), to create precise (±0.06 mm) 3-D animations of the quadrate, braincase, upper bill and mandible of three mallard ducks, *Anas platyrhynchos*. We defined a joint coordinate system (JCS) for the quadrato-squamosal joint with the axes aligned to the anatomical planes of the skull. In this coordinate system, the quadrate's 3-D rotations produce an elliptical path of pterygoid process motion, with medial and rostrodorsal then lateral and rostrodorsal motion as the upper bill elevates. As the upper bill depresses, the pterygoid process continues along the ellipsoidal path, with lateral and caudoventral then medial and caudoventral motion. We also found that the mandibular rami bow outwards (streptognathy) during mandibular depression, which may cause the lateral component of quadrate rotation that we observed. Relative to the JCS aligned with the anatomical planes of the skull, a second JCS aligned with quadrato-squamosal joint anatomy did not produce a simpler description of quadrate kinematics.

Supplementary material available online at http://jeb.biologists.org/cgi/content/full/214/12/2036/DC1

Key words: quadrate, kinematics, cranial kinesis, feeding, X-ray, XROMM, mallard, duck.

INTRODUCTION

Avian cranial kinesis was first described over 250 years ago (Hérissant, 1748). Since then, the mechanism, evolution, diversity and functions of avian cranial kinesis have been of great interest (e.g. Simonetta, 1960; Bock, 1964; Bühler, 1981; Zusi, 1984; van Gennip and Berkhoudt, 1992; Bout and Zweers, 2001; Gussekloo and Bout, 2005). Consensus on a general model of upper bill elevation has emerged in which the quadrate bone (Fig. 1) rotates rostrally, dorsally and slightly medially about the quadrato-squamosal joint, transferring force to the mobile pterygoid-palatine complex and jugal, which in turn push on the upper bill, causing it to elevate (Bock, 1964; Zusi, 1984; Gussekloo et al., 2001). There are several proposed functions of cranial kinesis, including, but not limited to: greater control of the jaws and gape, increased ability to feed selectively, shock absorbance, increased speed of opening and closing of the bills and reduced force necessary to open the bills (e.g. Bock, 1964; Zusi, 1967; Bout and Zweers, 2001; Gurd, 2006; Gurd, 2007; Estrella and Masero, 2007).

The quadrate is a keystone of cranial movement, as it articulates with the squamosal (braincase), pterygoid, jugal and mandible (Fig. 1). This makes its kinematics of particular interest. In most neognaths, the quadrate has a well-defined, bicondylar articulation with the squamosal (Cracraft, 1986; Elzanowski et al., 2000). Depending on the species, this quadrato-squamosal joint has been hypothesized to have one to three degrees of freedom (Bühler, 1981). In the mallard duck (*Anas platyrhynchos*), the two condyles of the otic process of the quadrate (Fig. 1D,E) are oriented such that a line passing through both condyles is oriented primarily mediolaterally, with a slight rostrocaudal tilt (Fig. 1B). From anatomical manipulation, Zweers (Zweers, 1974) found that the quadrate in mallard ducks can potentially rotate around multiple axes, including rostrocaudal and mediolateral rotation about the otic process of the quadrate at its articulation with the squamosal (Zweers, 1974).

Because quadrate movements are not visible externally, three-dimensional (3-D) X-ray motion analysis is required to test hypotheses of quadrate kinematics. Gussekloo et al. (Gussekloo et al., 2001) used an innovative 3-D X-ray imaging technique (Roentegen stereophotogrammetry) to measure quadrate movement during postmortem manipulation of the upper bill in two neognaths (a crow and a knot) and three paleognaths (an ostrich, an emu and a rhea). Their study concluded that the quadrate rotates primarily rostrocaudally, with little medial or lateral movement, and also found some rotation about a longitudinal axis running through the quadrate. These experiments analyzed movement by manipulating the upper bill, which may not have accurately recreated *in vivo* kinematics as the forces applied do not include muscular forces. The authors suggest that there could be more medial movement of the quadrate if the protractor quadrati muscle were active. Therefore, dynamic measurement of 3-D quadrate, upper bill and lower bill kinematics *in vivo* would provide an improved description of cranial kinesis in birds.

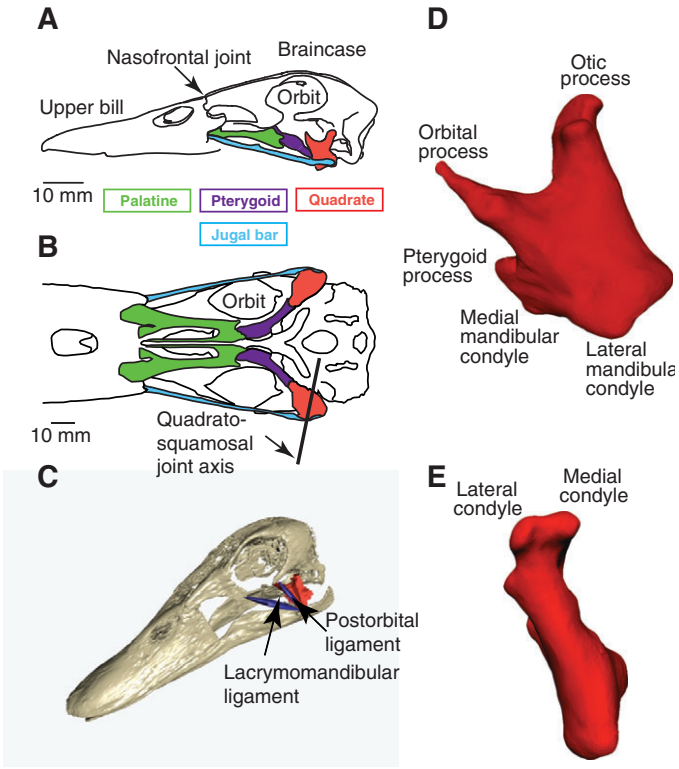

Fig. 1. Mallard skull and quadrate anatomy. (A) Lateral view. The bones involved in cranial kinesis are labeled: the quadrate in red, the pterygoid in purple, the palatine in green, the jugal in blue and the upper bill. Rotation of the upper bill occurs about the nasofrontal joint. (B) Ventral view. The long axis of the quadrato-squamosal joint passes through the two condyles of the otic process of the quadrate. (C) Surface mesh model of skull with ligaments relevant to coupled kinesis. The quadrate is in red and the two ligaments are in blue. (D) Surface mesh model of a left quadrate, lateral view. This 3-D model is a composite from a CT scan of the body of the quadrate and a higher-resolution laser scan of the otic process. (E) Posterior view of the quadrate showing the lateral and medial condyles of the otic process.

The kinematics of the lower bill may not be independent from the quadrate and upper bill system. The coupled kinesis hypothesis proposes that the upper bill and lower bill are linked such that the upper bill must elevate before the lower bill can depress (e.g. Bock, 1964; Zusi, 1967). Several mechanical hypotheses have been proposed to explain coupled kinesis, including the presence of stiff ligaments between the skull and mandible (Bock, 1964), an interlocking jaw joint (Bock, 1964; Zusi, 1967) and simultaneous activity of jaw opening and jaw closing muscles (Bühler, 1981). The presence and robustness of the ligaments potentially involved in coupled kinesis is variable, but the postorbital or the lacrymomandibular, particularly in anatids, are the most cited (Fig. 1C). The mechanism is described fully by Bock (Bock, 1964) and Zusi (Zusi, 1967) among others, but briefly, when the mandible begins to depress, it is stopped because of an inelastic ligament. For the mandible to depress further, the quadrate must swing forward, protracting the mandible and thus reducing the tension on the ligament (Bock, 1964; Zusi, 1967).

Coupled kinesis *via* ligaments is controversial and experiments have yielded varying results (Hoese and Westneat, 1996; Bout and Zweers, 2001; Nuijens et al., 2000). Bout and Zweers (Bout and Zweers, 2001) found that the postorbital and lacrymomandibular ligaments do not provide enough resistance to prevent the lower bill from depressing in several species, including mallards. However, in his study of the mallard feeding apparatus with cinematography and electromyography, Zweers (Zweers, 1974) used the postorbital and lacrymomandibular ligaments to help explain mandible and quadrate kinematics. Zusi (Zusi, 1967) performed an *in situ* experiment, in which he stimulated the depressor mandibulae muscle of a chicken (*Gallus domesticus*), which has a robust postorbital ligament, and a grosbeak (*Hesperiphona verpertina*), which has a weak postorbital ligament. He found that even with the postorbital ligaments cut, the upper and lower jaw moved together, though less so than with intact ligaments, leading him to conclude that the quadrato-mandibular articulation contributes to the coordinated movement through the depressor mandibulae muscle. Zusi suggested that in order to disengage the coupling mechanism, the rami of the mandible must spread laterally and move posteriorly or the quadrate must move rostromedially.

Here we use marker-based X-ray reconstruction of moving morphology (XROMM) (Brainerd et al., 2010) to measure quadrate, braincase, upper bill and mandible kinematics *in vivo* during feeding in the mallard. XROMM animations combine precise (±0.1 mm) bone kinematics from biplanar X-ray videos with high-resolution bone morphology from a 3-D bone scan. The bone morphology can be used to create repeatable joint coordinate systems for quantifying joint motion with six degrees of freedom, and animation of the whole bone makes it possible to track any point on the bones in an XROMM animation. The present study focuses on the kinematics of the quadrate and its interactions with the upper and lower bills. We also explore two different coordinate systems to describe quadrate motion, one based on quadrato-squamosal joint anatomy and one based on the anatomical planes of the skull.

MATERIALS AND METHODS

Data collection

Three adult female domestic mallard ducks, *Anas platyrhynchos* (Linnaeus 1758), were used in this study. All animal care and experimental procedures were approved by the Institutional Animal Care and Use Committee of Brown University.

We used marker-based XROMM to create 3-D animations of the quadrate, braincase, upper bill and mandible of three *A. platyrhynchos* [see Brainerd et al. (Brainerd et al., 2010) for XROMM equipment and software details]. Briefly, we surgically implanted a minimum of three metal markers each in the quadrate, mandible, upper bill and braincase (Fig. 2). We implanted markers on the left side of the head for all birds. To implant each marker, birds were anaesthetized with isoflurane in O_2. Anesthesia was induced using a custom constructed facemask and then maintained for the duration of the surgery through an endotracheal tube. Feathers overlying the implantation site were removed and a small cutaneous incision was made. Connective tissue and muscle were incised or reflected and a hand drill with a bit diameter the same as the marker was used to drill a small hole in the bone. Finally, a marker (Baltec, Los Angeles, CA, USA) was manually pressed in the hole and all tissues were sutured closed. On the bills, we used a small amount of cyanoacrylate tissue glue (Vetbond Tissue Adhesive, 3M, St Paul, MN, USA) to close the holes. Markers were spaced as far apart as possible to maximize the accuracy of bone animations (Brainerd et al., 2010). The ducks fed and behaved normally a few hours after surgery, but were allowed to recover for at least 2 days before the start of data recording. They received analgesic immediately before and after surgery and continued to feed and behave normally with no further pain relief. For earlier surgeries in our experiment, we

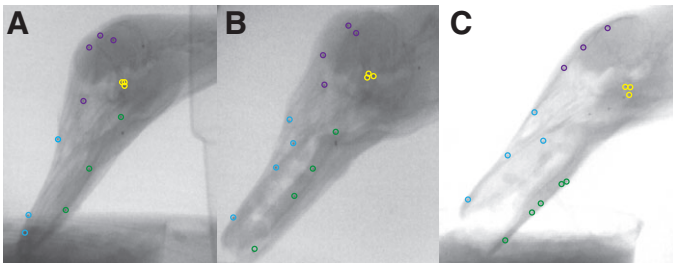

Fig. 2. Marker locations in the three individual ducks in this study: (A) Duck A; (B) Duck B; and (C) Duck C. Yellow circles, quadrate markers; blue circles, upper bill markers; green circles, mandible markers; purple circles, braincase markers. Ducks A and B both have markers in the hyoid that were not analyzed for this study. Duck C has markers in the jugal that were not analyzed for this study. Note the close placement of the quadrate markers, as explained in the Materials and methods.

used 1 mm diameter spherical stainless steel markers (Ducks A and B) whereas in later surgeries we used 0.8 mm diameter spherical tantalum markers (Duck C).

To capture the movement of the marked bones, we used two mobile C-arm fluoroscopes (OEC Model 9400; C-arms refurbished and retrofitted by Radiological Imaging Services, Hamburg, PA, USA) retrofitted with two high-speed video cameras (Photron Fastcam 1024 PCI, Intronix Imaging Technologies, Westlake Village, CA, USA). We positioned the fluoroscopes such that their beams crossed, creating a small volume where movement in both views could be captured. All of the videos were recorded at 250 frames s^{-1}. To remove distortion, we placed a punched steel grid over each image intensifier and took an image to create a de-distortion matrix in MATLAB version R2006a (The MathWorks, Inc., Natick, MA, USA) that we then applied to the digital videos (Brainerd et al., 2010). We calibrated the space before and after each filming session by placing a 3-D calibration object into the space where the beams crossed and images were recorded (Brainerd et al., 2010).

Mallards are omnivores; vegetation makes up most of their diet, but they will also eat insects and insect larvae (Goodman and Fisher, 1962). Typically, they filter food from the water or nip with the tip of the bill. Ducks in our study were fed pelleted duck food in water (supplementary material Movie 1). The mean diameter of the cylindrical food pellets was 8 mm and the length 5 mm. We handled the ducks frequently prior to surgery, and trained them to eat while their bodies were restrained in a plastic box. During filming, the ducks were positioned on a feeding platform so that they could easily reach the food. The ducks generally ate for approximately 25 s in each trial.

After approximately 2 weeks of data collection, the ducks were killed and computed tomography (CT) scans (Philips Medical System, Best, The Netherlands) of the heads were made at Rhode Island Hospital at 1024×1024 image resolution, a field of view size of 100 mm and a slice thickness of 0.625 mm. Amira 4.0 (Visage Imaging, Inc., San Diego, CA, USA) was used to create polygonal mesh surface models of the marked bones and metal markers, resulting in a 3-D mesh surface model of each bone and the positions of the markers relative to the bones.

Marker tracking and XROMM animation

Marker positions were digitized and reconstructed in 3-D using the program XrayProject 2.0 in MATLAB (Brainerd et al., 2010). Precision of marker tracking was measured by calculating the mean of the standard deviation of the distances between all pairs of markers collocated in each bone (Tashman and Anderst, 2003; Brainerd et al., 2010).

To produce XROMM animations, the time series of *X*-, *Y*- and *Z*-coordinates for the markers were first filtered in MATLAB with a Butterworth low-pass filter (frequency cutoff 25 Hz). In XrayProject 2.0, the markers for each bone were collected into marker sets, and singular value decomposition (SVD) was used to calculate the rigid body transformation between the CT position of each marker set and the position of the corresponding marker set in the first frame of X-ray video (Söderkvist and Wedin, 1993). The calculated rigid body transformations for the marker sets were then applied to the 3-D bone models from CT scans in Maya animation software (Autodesk, San Rafael, CA, USA).

Joint coordinate systems

To express movement of the bones in an anatomically meaningful way, we created joint coordinate systems (JCSs) for the nasofrontal (N), quadrato-squamosal (Q) and quadrato-mandibular (M) articulations (Fig. 3). A JCS is created in Maya by aligning 3-D axes to skeletal landmarks (Brainerd et al., 2010). First, an anatomical coordinate system (ACS) is oriented to the distal bone and attached. The ACS is then duplicated and the copy is attached

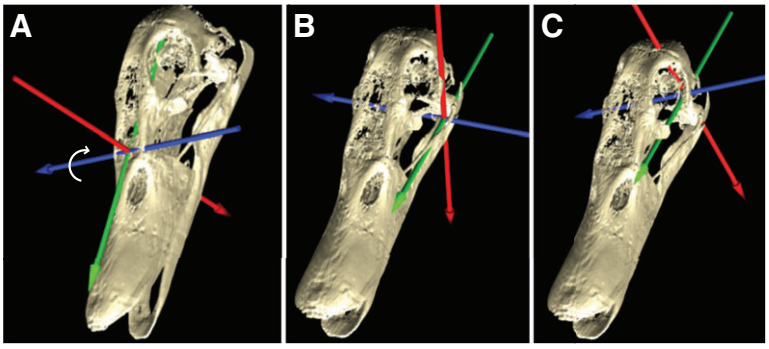

Fig. 3. Joint coordinate systems (JCSs) for nasofrontal, quadrato-squamosal and quadrato-mandibular joints. The *X*-axis is red, the *Y*-axis is green and the *Z*-axis is blue. The arrowheads indicate the polarity of the rotation according to the right-hand rule, and the axes define three potential joint rotations, hereafter abbreviated rx, ry and rz. (A) Nasofrontal (N) coordinate system. Positive rotation of the nasofrontal joint about the *Z*-axis (i.e. positive N_{rz}) corresponds to upper bill elevation (white arrow). (B) Mandibular (M) coordinate system for the quadrato-mandibular joint. Positive M_{rz} corresponds to lower bill elevation. (C) Quadrate (Q) coordinate system for the quadrato-squamosal joint in the anatomical planes of the skull. Positive Q_{rz} corresponds to rostral rotation of the quadrate. Positive Q_{ry} corresponds to lateral rotation. Positive Q_{rx} corresponds to counterclockwise rotation of the left quadrate in ventral view (internal rotation).

Table 1. Polarity of rotations and anatomical movements

Rotation	N_{rz}	M_{rz}	Q_{rx}	Q_{ry}	Q_{rz}
Positive	Elevation	Elevation	Counterclockwise*	Lateral	Rostral
Negative	Depression	Depression	Clockwise*	Medial	Caudal

M_{rz}, mandibular rotation about the *Z*-axis; N_{rz}, nasofrontal rotation about the *Z*-axis; Q_{rx}, quadrate rotation about the *X*-axis; Q_{ry}, quadrate rotation about the *Y*-axis; Q_{rz}, quadrate rotation about the *Z*-axis. N_{ry}, N_{rx}, M_{ry} and M_{rx} were not included in the analysis as they did not show substantial rotation.
*Viewed from a ventral perspective, left quadrate.

to the proximal bone. An explicit hierarchy of ordered rotations is selected, which, combined with the proximal and distal ACSs, specify the JCS. The axes follow the motion of the two bones in the XROMM animation and output three ordered rotations and three translations (six degree of freedom joint kinematics) of the bone of interest, relative to the proximal bone (supplementary material Movie 2).

Joint motion can be explored by placing various JCSs and comparing the resulting six degree of freedom joint kinematics. An advantage of the XROMM method is that XROMM animations contain both 3-D motion and 3-D bone morphology (Gatesy et al., 2010). The 3-D bone morphology can be used to place JCSs reliably and repeatably (Brainerd et al., 2010; Gatesy et al., 2010). We placed three primary JCSs for each duck, on the nasofrontal, quadrato-mandibular and quadrato-squamosal joints (Fig. 3). For the quadrato-squamosal joint, we created two JCSs, one oriented to the anatomy of the quadrato-squamosal joint (Fig. 1) and the other oriented to the anatomical planes of the skull (Fig. 3).

In our nasofrontal JCS, the *Z*-axis runs parallel to and passes through the long axis of the nasofrontal joint (Fig. 3A). Rotation about the *Z*-axis (N_{rz}) measures upper bill pitch, which corresponds to elevation and depression (Table 1). The *Y*-axis is oriented parallel to the upper bill and the *X*-axis is perpendicular to the *Z*- and *Y*-axes. Rotations about the *X*- and *Y*-axes are expected to be small in this hinge-like joint, but they would measure yaw and roll of the upper bill, respectively, relative to the braincase.

For the quadrato-mandibular joint, the *Z*-axis passes through the medial and lateral mandibular condyles of the quadrate (Fig. 3B). We chose to use the quadrate as the proximal bone rather than the skull as we are currently interested in quadrate kinematics and their impact on other bones. It is therefore important to note that the mandible movements we report are relative to the quadrate, not the braincase. Rotation about the *Z*-axis (M_{rz}) measures the elevation and depression of the mandible relative to the quadrate (Table 1).

For the quadrato-squamosal JCS aligned to the anatomical planes of the skull, the *Z*-axis is oriented mediolaterally relative to the braincase and passes through the otic process of the quadrate (Fig. 3C). Rotation about the *Z*-axis (Q_{rz}) measures rostral and caudal rotation of the quadrate. The *Y*-axis lies in a sagittal plane of the skull and the *X*-axis lies in a transverse plane of the skull. The *Y*-axis measures medial and lateral rotation (Q_{ry}) of the quadrate. The *X*-axis runs dorsoventrally through the body of the quadrate. Looking from a ventral perspective, Q_{rx} can be thought of as counterclockwise (positive) and clockwise (negative) rotation of the body of the left quadrate (Table 1).

For the JCS oriented to the anatomy of the quadrato-squamosal joint, the *Z*-axis is set to pass through the two condyles of the otic process of the quadrate (Fig. 1E) along the quadrato-squamosal joint axis (Fig. 1B). Because the orientation of this JCS is oblique to the skull, rotation about the *Z*-axis produces a mixture of rostrocaudal and mediolateral quadrate movement. The *Y*-axis was aligned to pass through the tip of the orbital process of the quadrate, and the *X*-axis runs through the body of the quadrate. We created this JCS to explore whether we could use the anatomy of the quadrato-squamosal joint to find a single axis that describes the majority of quadrate rotation, with fewer necessary degrees of freedom than the JCS that we aligned to the anatomical planes of the skull.

We set the zero values for the JCSs at a time point when the jaws appeared to be maximally closed. Because we used one trial for each duck to set the axes, the zero position of the axes did not always match perfectly with maximal jaw closure when applied to a different trial, even though we used the same models and markers for each trial. This should not impact our analysis as we measured differences between peaks and the overall shape of the graphs rather than magnitudes read directly from the graphs.

When calculating rotations about three orthogonal axes, the order in which the rotations are calculated, i.e. the hierarchy of ordered rotations, will potentially affect the values for the three rotations (Zatsiorsky, 1998). If the *Z*-axis rotation is calculated first, then *Y* and then *X*, the values for these rotations will be different relative to a system where the *X*-axis rotation is calculated first, followed by *Y* and *Z* (i.e. *Z*,*Y*,*X versus X*,*Y*,*Z* rotation order) even though the starting position and the final position are the same. Maya actually uses a different notation to signify rotation order. In Maya, a *Z*,*Y*,*X* rotation order calculates *X* first, then *Y* then *Z*. We chose not to use this notation as it is more typical to put the rotation calculated first as the first listed (Zatsiorsky, 1998). To determine whether the hierarchy of ordered rotations would appreciably affect our results, we calculated rotations for both the *Z*,*Y*,*X* (*Z* calculated first) and *X*,*Y*,*Z* (*X* calculated first) rotation orders for one trial. We did not change the orientation of the axes for these calculations. We found little effect of rotation order (supplementary material Fig. S1) and used *Z*,*Y*,*X* as the rotation order for this study. For all of the JCSs, we oriented the ACS such that the largest expected rotation was captured by the *Z*-axis, which is the first rotation calculated in the hierarchy. For example, N_{rz} captures most of the motion at the nasofrontal joint (Fig. 4).

Statistics

The JCS rotations and translations were exported from Maya for analysis in IGOR Pro v5.0 and 6.0 (WaveMetrics, Lake Oswego, OR, USA). In IGOR Pro, we measured the minimum and maximum rotations about the *Z*-axis of the mandible and upper bill, all three rotations of the quadrate and the duration of each cycle. A cycle was defined as the period of time from maximum upper bill depression to maximum elevation to maximum depression again. We analyzed two trials from Duck A, four trials from Duck B and two trials from Duck C. The number of cycles per trial varied from 13 to 51 depending on how much of the video was analyzable (i.e. at least three markers were visible in each bone).

To measure the similarity in timing and shape of nasofrontal, mandibular and quadrate rotation waveforms, we used cross correlations to calculate the lag time and correlation coefficient between pairs of waveforms. Cross correlation is a signal processing

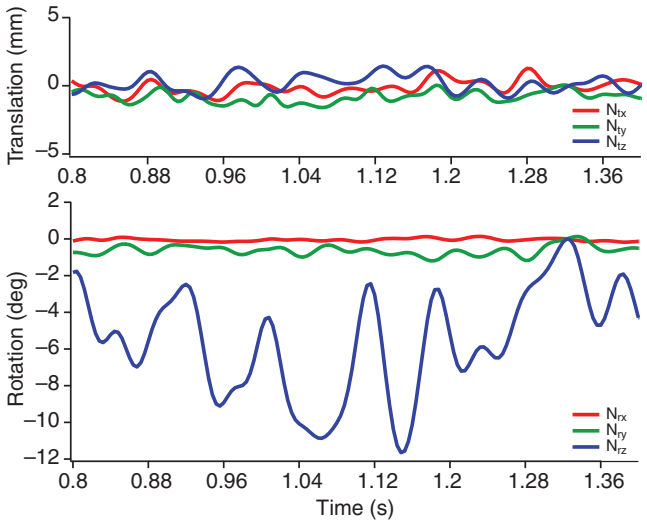

Fig. 4. Six degree of freedom kinematics as measured by the JCS on the nasofrontal joint (Fig. 3A). Most of the motion is captured as rotation about the *Z*-axis (N_{rz}). All other rotations and translations are relatively small, indicating that the nasofrontal joint acts as a classical hinge joint.

technique that has been used in a variety of fields, including kinematics (Green et al., 2000; Bishop, 2006), electromyography studies (Moore, 1993; Wren et al., 2006) and neurobiology (Shao and Tsau, 1996). From each trial we chose 10 consecutive cycles of feeding to analyze based on the regularity of the movement, i.e. we deliberately chose sections with the most sinusoidal movements (but see supplementary material Fig. S2 for an example of more irregular motion).

Cross correlation provides a way to look at time displacement (the lag) and spatial pattern (the correlation coefficient) between two waveforms. Our customized MATLAB script used the function xcov to calculate a normalized cross covariance, which is equivalent to a correlation (Rodgers and Nicewander, 1988). The normalization process subtracts the mean and divides by the variance, which gives a correlation coefficient that ranges from –1 to 1, allowing us to compare correlations across sequences. When the lag time was zero, we used the correlation coefficient directly from the cross covariance. When there was a lag, we realigned the kinematic waveforms to remove the lag and calculated the correlation coefficient again to compare the shape of the curves more closely.

RESULTS

General observations of feeding behavior

The general sequence of feeding behaviors we observed was similar to that reported by Zweers (Zweers, 1974) for mallards straining food from water. We found that the ducks typically gather food from the water using rapid bill movements, during which the jaws open and close with some variation in the amplitude of the motions (Table 2, Fig. 4). The head moves back and forth in a throwing motion as the food travels through the mouth during this food collection phase. Once the oral pharynx is full of food, the duck lifts its head away from the food dish and continues to use a combination of lingual and inertial transport (as evaluated from fluoroscopic videos) with moderate opening and closing of both bills as the food is transported to the esophagus (supplementary material Movie 1). The feeding sequences we selected for analysis were mainly during continuous food gathering behavior, with some food transport.

Precision of marker tracking

The mean of the mean standard deviation between marker pairs within the same bone was 0.058 mm across all ducks and trials (see Table 3 for the mean standard deviation of pairwise marker distances for each trial). These results indicate an overall marker tracking precision for this study of ±0.06 mm.

In Duck C we found that pairwise distances between marker pairs located on the opposite sides of the mandible had statistically significantly greater standard deviations than marker pairs on the same side of the mandible (0.46 mm *versus* 0.07 mm in trial 1, $P<0.0004$; and 0.52 mm *versus* 0.09 mm in trial 2, $P<0.0002$, respectively). This suggests that there is movement between the two rami of the mandible, so we did not use marker pairs on opposite sides of the mandible to calculate the marker tracking precisions for Duck C shown in Table 3. For Ducks A and B, there were nine pairs used to calculate the mean change in distance between pairs of markers collocated in the same bone and 10 pairs for Duck C.

Upper bill kinematics

Our joint coordinate systems for the nasofrontal, quadrato-squamosal and quadrato-mandibular joints (Fig. 3) generate six degree of freedom descriptions of joint movement in anatomically meaningful frames of reference (Fig. 4). For the nasofrontal joint, we found that upper bill movement can be quantified primarily as rotation about the *Z*-axis (N_{rz}), with little contribution from the other five degrees of freedom (N_{rx}, N_{ry}, N_{tx}, N_{ty} and N_{tz}). Thus, the nasofrontal articulation acts as a hinge joint, with rotation about just one axis and little or no translation at the joint (Fig. 4).

Positive N_{rz} corresponds to upper bill elevation and negative N_{rz} corresponds to upper bill depression (Table 1, Fig. 3A). Mean upper bill elevation for each of the eight feeding trials (with 235 total cycles analyzed) ranged from 4.6±0.60 to 9.7±0.82 deg with a typical value of approximately 7 deg over all of the cycles in all feeding sequences (Table 2).

Mandible kinematics

In one of the individuals (Duck C), markers were placed on both sides of the mandible. The distance between these markers changed

Table 2. Mean ± s.d. of feeding cycle duration and maximum bill rotation in mallards, *Anas platyrhynchos*

Individual	Trial number	Number of cycles	Feeding cycle duration (s)	Max upper bill angle (deg)	Max lower bill angle (deg)
Duck A	1	22	0.078±0.004	4.58±0.6	–10.52±1.39
Duck A	2	51	0.078±0.002	7.82±0.4	–15.91±7.4
Duck B	1	51	0.088±0.003	8.14±0.61	–11.56±0.82
Duck B	2	28	0.078±0.004	7.83±0.84	–10.5±1.07
Duck B	3	33	0.087±0.004	6.91±0.76	–11.32±0.94
Duck B	4	27	0.092±0.004	9.68±0.82	–11.95±1.07
Duck C	1	17	0.066±0.005	4.97±0.86	–7.18±4.6
Duck C	2	13	0.062±0.006	6.54±0.98	–10.9±5.43

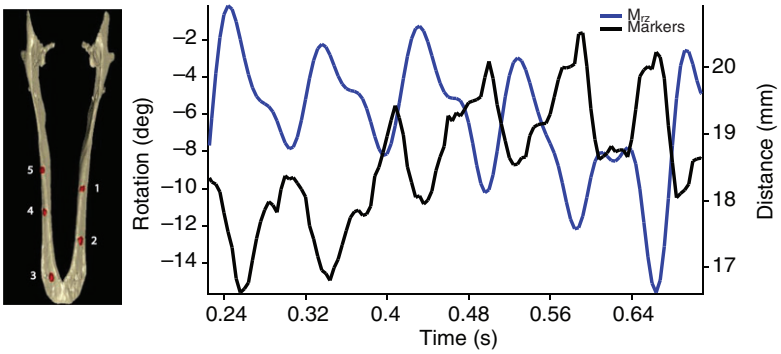

Fig. 5. Deformation of the lower bill during feeding. Left: mandible with locations of the five tantalum markers; right: mandibular depression and elevation (mandible, blue line; positive rotation corresponds to mandibular elevation), and the straight-line distance between two markers (1 and 5) on the opposite sides of the mandible. Note that the distance between markers 1 and 5 varies from 18 to nearly 21 mm, with the maximum spreading of the mandibular rami occurring at maximum lower jaw depression.

by nearly 3 mm, in phase with mandibular depression and elevation such that the maximum intermarker distance occurred during maximum jaw opening (Fig. 5). We confirmed this result by looking at dorsal X-ray movie views of other individual ducks in which the unmarked rami can be seen spreading apart during jaw opening. This is an interesting finding, but potentially confounding to the generation of our XROMM animation of the mandible, as it violates the assumption of a rigid body used in our transform calculations. In our animations, the quadrato-mandibular joint does not always stay articulated, likely because we did not attempt to animate a flexible mandible model. Additionally, the markers in the mandible were arranged in roughly a straight line, which reduces the accuracy of the rotation matrix (Söderkvist and Wedin, 1993) for the ducks with markers on only one side of the mandible, Duck A and Duck B. We believe that our *Z*-axis rotation (M_{rz}) gives a reliable estimate of mandible depression and elevation at the quadrato-mandibular joint. However, we are unsure about the accuracy of the other rotations and translations. Therefore, we treat the quadrato-mandibular articulation as a hinge joint with one degree of freedom, but it should be recognized that this joint may have more degrees of freedom than we are currently able to detect.

Our mandibular axis system measured mandibular movement relative to the quadrate. Positive M_{rz} corresponds to lower bill elevation and negative M_{rz} corresponds to lower bill depression (Table 1, Fig. 3B). Mean lower bill depression for each of the eight feeding trials ranged from –7.2±4.60 to –15.9±7.40 deg, with most trials showing a typical value of approximately 11 deg (Table 2).

Quadrate kinematics

We found that quadrate movement is substantially more complex than upper and lower bill movements. Given the tightly conforming morphology of the quadrato-squamosal joint, we did not expect to measure substantial quadrate translation utilizing a JCS that passes through the otic process of the quadrate at this articulation. Indeed, the observed translations were small (of the order of 1 mm or less), so we concentrate here on the rotations about three axes aligned with the anatomical planes of the braincase (Fig. 3C, Table 1).

Table 3. Marker tracking precision in mallards

Individual	Trial number	Mean pairwise s.d. (mm)
Duck A	1	0.048
Duck A	2	0.051
Duck B	1	0.049
Duck B	2	0.052
Duck B	3	0.052
Duck B	4	0.052
Duck C	1	0.070
Duck C	2	0.090

For our JCS in the anatomical planes of the skull, we found substantial rotations about all three quadrate axes (Q_{rx}, Q_{ry} and Q_{rz}; Fig. 6B). These three components of rotation are all fairly closely correlated in time with upper bill elevation, N_{rz}, and lower bill depression, M_{rz} (Fig. 6A). Substantial motion around all three quadrato-squamosal joint axes suggests a complex, 3-D motion that includes rostrocaudal rotation of the quadrate in a parasagittal plane about a mediolaterally oriented axis (Q_{rz}), mediolateral motion about a rostrocaudally oriented axis and rotation of the quadrate about a center axis running dorsoventrally through the bone (Q_{rx}).

Our JCS aligned to the quadrato-squamosal joint did not capture the quadrate's movements with fewer degrees of freedom. We found substantial rotation about all three axes (Fig. 7), with similar complexity to our JCS based on the anatomical planes of the skull.

Cross-correlation analysis

As a visualization aid, we plotted the three quadrate rotations (from our JCS based on the anatomical planes; Fig. 3C) *versus* rotation at

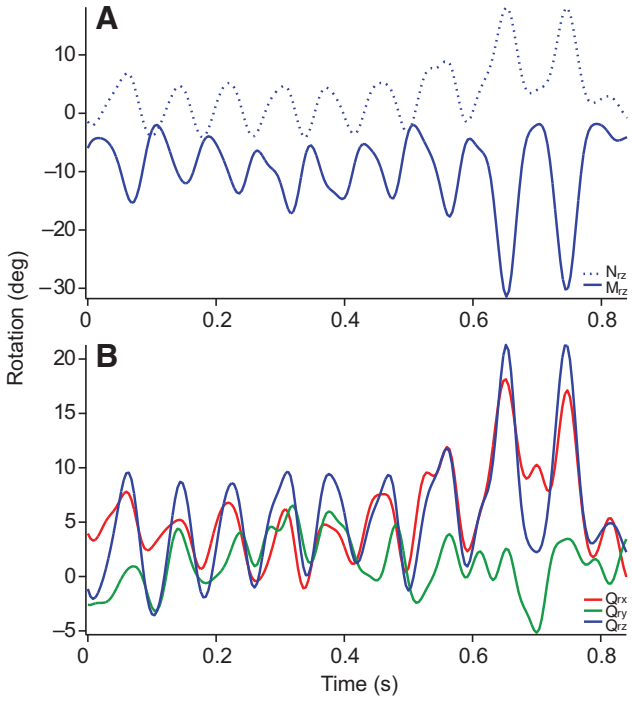

Fig. 6. Ten consecutive feeding cycles from Duck A. Only the primary rotations of interest are shown. (A) Upper bill elevation and depression at the nasofrontal joint about the *Z*-axis (N_{rz}) and mandibular depression and elevation at the quadrato-mandibular joint (M_{rz}). (B) All three rotations of the quadrate at the quadrato-squamosal joint (Q_{rx}, Q_{ry} and Q_{rz}). See Fig. 3 for JCS conventions.

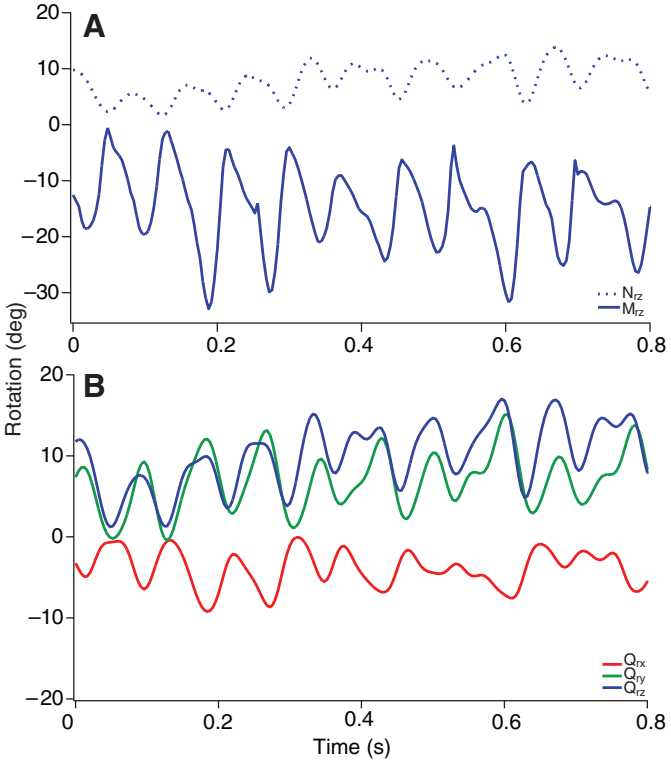

Fig. 7. Ten consecutive feeding cycles from Duck A using a quadrato-squamosal JCS aligned to quadrate joint anatomy. The *Z*-axis passes through the medial and lateral condyles of the otic process of the quadrate, such that Q_{rz} quantifies rotation about the axis drawn in Fig. 1B. (A) Upper bill elevation and depression at the nasofrontal joint about the *Z*-axis (N_{rz}) and mandibular depression and elevation at the quadrato-mandibular joint (M_{rz}). (B) All three rotations of the quadrate (Q_{rx}, Q_{ry} and Q_{rz}). Notice the similar magnitudes of rotation about all three quadrato-squamosal axes.

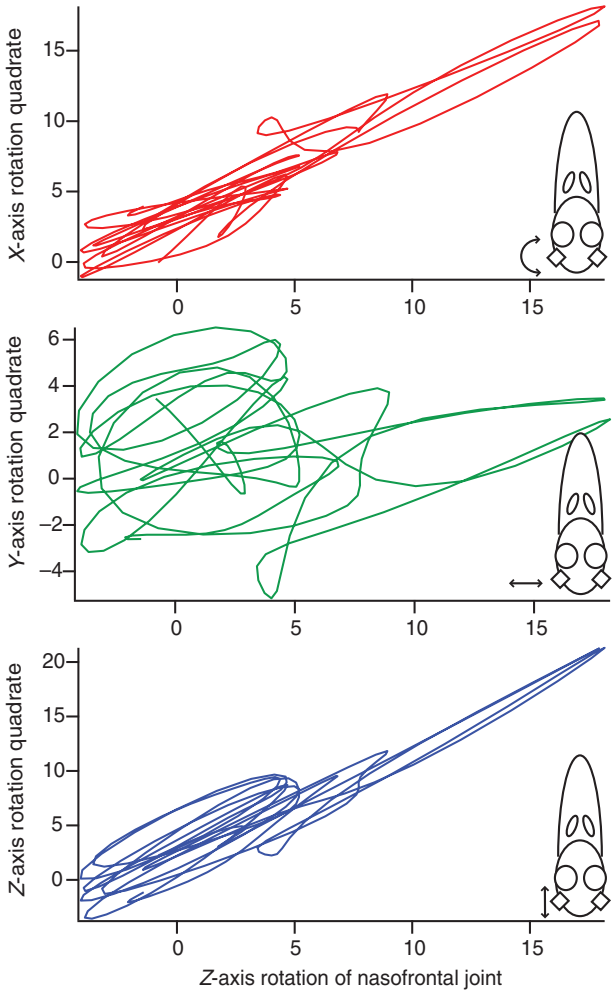

Fig. 8. Rotations of the quadrate (Q_{rx}, Q_{ry} and Q_{rz}) relative to depression and elevation of the upper bill at the nasofrontal joint (N_{rz}) over 10 consecutive feeding cycles. Notice that the quadrate *Z*-axis and *X*-axis rotation loops are tighter than the quadrate *Y*-axis rotation loops. The small diagrams indicate the primary motion of the quadrate that would be produced by each of these isolated rotations. The loop graphs were created from the same sequence of 10 cycles shown in Fig. 6.

the nasofrontal joint for 10 consecutive cycles (Fig. 8). These plots create loops that display how closely correlated the quadrate rotations are to upper bill elevation. We used cross-correlation analysis to quantify the similarity in timing and waveform shape between pairs of rotation waveforms from our JCS analyses (Fig. 9).

Most of the pairwise cross-correlations of waveforms resulted in lag times that were consistently positive or negative (Fig. 9A). As expected from visual inspection of waveforms (Fig. 6), mean lag times were small (–0.003±0.002 s) between upper bill rotation at the nasofrontal joint and quadrate *Z*-axis rotation ($N\times Q_{rz}$). There was a consistently negative and relatively long lag for $N\times Q_{ry}$ (–0.013±0.006 s).

Mandibular rotation at the quadrato-mandibular joint lagged behind nasofrontal joint rotation in all eight trials ($N\times M$, Fig. 9A), with a mean lag of –0.01±0.004 s (i.e. lower bill depression lagged behind upper bill elevation by a mean of 10 ms). Mandibular *Z*-axis rotation and quadrate *Z*-axis rotation had consistently positive lag times (mean 0.006±0.003). Lag times were also consistently small, 0.001±0.003 s on average, between mandibular *Z*-axis rotation and quadrate *Y*-axis rotation ($M\times Q_{ry}$). However, for both $M\times Q_{ry}$ and $M\times Q_{rx}$ (mean 0.001±0.013), some sequences showed a negative lag time whereas others were positive or zero (Fig. 9A).

The normalized correlation coefficient is a measure of the similarity in shape between two waveforms. As suggested by the phase graphs (Fig. 8), the strongest correlations were $N\times Q_{rz}$ and $N\times Q_{rx}$, with means ± s.d. of 0.93±0.06 and 0.85±0.14, respectively (Fig. 9B). Nasofrontal and mandibular rotations ($N\times M$) are negatively correlated, with a mean of –0.71±0.21. The $N\times Q_{ry}$ correlations were found to be not significant in two of the eight trials ($P>0.05$). These two correlations have been excluded from Fig. 9 and all means.

We also ran cross-correlation analysis for our JCS oriented to quadrate anatomy (Fig. 1B). This JCS shows a higher correlation between quadrate *Y*-axis rotation and mandibular depression (Table 4). There was also a weaker correlation between quadrate *X*-axis rotation and nasofrontal elevation.

As mentioned above, we deliberately selected sections of data for this cross-correlation analysis that showed the most consistent sinusoidal motions of the upper and lower bills. In other sections of the feeding trials, the relationship between upper and lower bill motion were more complex and variable (supplementary material Fig. S2).

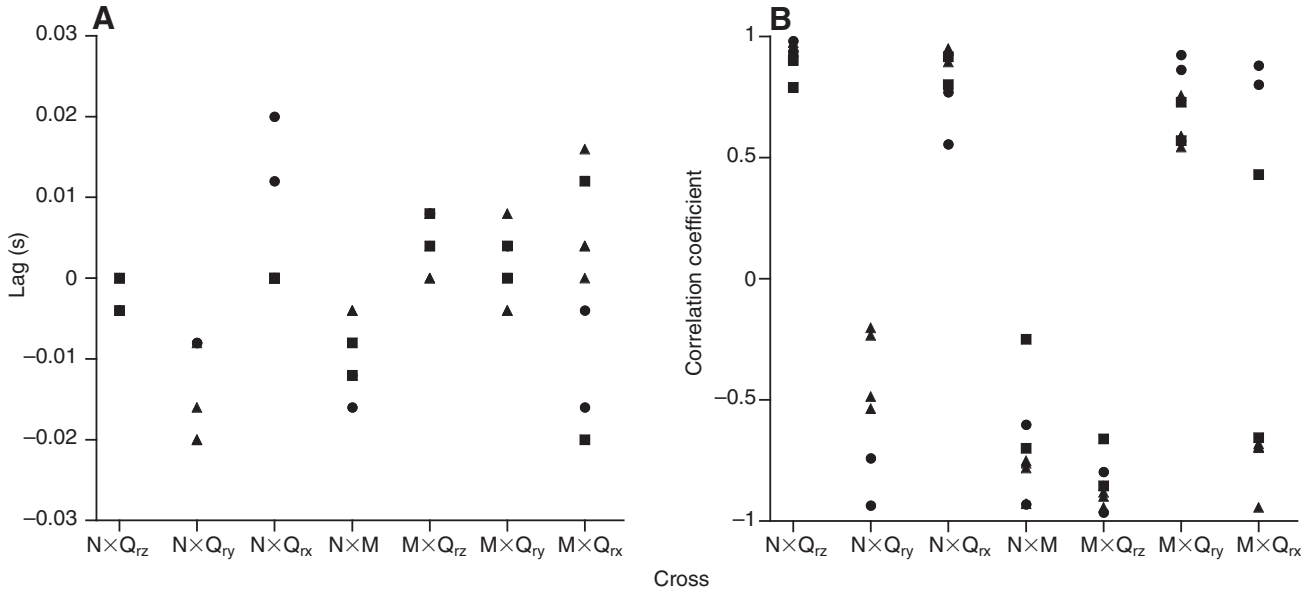

Fig. 9. Lag times and correlation coefficients for cross correlations between upper bill rotation at the nasofrontal hinge (N), mandibular depression and elevation (M), and the three quadrato-squamosal rotations (Q_{rz}, Q_{ry} and Q_{rx}) for the quadrate JCS aligned to the planes of the skull. (A) Lag times. Lag time indicates the time shift required to maximize the correlation coefficient for each pair of kinematic curves. A negative lag time indicates that the waveform listed first precedes the waveform listed second, e.g. a negative value for N×Q_{ry} indicates that Q_{ry} lags behind nasofrontal joint rotation. (B) Correlation coefficients. Tightly clustered points indicate strong similarity in the shape of the kinematic curves, with –1 indicating opposite polarity of rotation (as set by the joint coordinate systems, Fig. 3). × indicates the cross-correlation, such that N×Q_{rz} is the lag time between upper bill elevation and depression (N) and the *Z*-axis rotation of the quadrate (Q_{rz}). Duck A, circles; Duck B, triangles; Duck C, squares. The points represent six to eight feeding trials per correlation, depending on how many of the cross-correlations were statistically significant. The frame rate was 250 frames s^{-1} (0.004 s temporal resolution for the lag times).

Translation of the pterygoid process

Affixing a point to the pterygoid process and tracking that point over time yields an obliquely oriented elliptical path, with the direction of motion being clockwise for a left quadrate when viewed in ventral or anterior perspective (Fig. 10). Starting from the most caudal location in each cycle, the point moves medial and rostrodorsal, then lateral and rostrodorsal, then lateral and caudoventral and then medial and caudoventral to return to approximately the starting point (Fig. 10). These complex motions result from the sum of rostrocaudal, mediolateral and quadrate axis rotations described by our quadrato-squamosal JCS (Fig. 3C, Fig. 6).

DISCUSSION

Previous studies of quadrate movement during feeding in birds have suggested that the quadrate rotates primarily about one axis, swinging in a rostral or rostromedial direction toward the pterygoid, thereby elevating the upper bill (e.g. Bock, 1964; Gussekloo et al., 2001). Our XROMM results from mallards feeding *in vivo* show greater complexity in quadrate motions, as shown by the 3-D rotational patterns and the elliptical pathway of the pterygoid process (Figs 6, 10). With a quadrato-squamosal JCS oriented to the anatomical planes of the skull, we found significant rotation about all three axes of the quadrato-squamosal joint (Fig. 6). Orienting the JCS to align with quadrato-squamosal joint anatomy does not reduce the complexity of the motion (Fig. 7). The pterygoid process does indeed move rostromedially during the first part of upper bill elevation, but then it moves rostrolaterally during the second half of upper bill elevation (Fig. 10B). Substantial dorsoventral movement of the pterygoid process also occurs (Fig. 10A). We also found, unexpectedly, that the mandible bows during depression (streptognathy), which may produce a lateral pull on the quadrate and contribute to the lateral quadrate movement during the second half of upper bill elevation. Alternatively, the lateral rotation of the

Table 4. Comparison of cross-correlation coefficients (mean ± 1 s.d.) between the joint coordinate system (JCS) oriented to anatomical planes of the skull (skull) and the JCS based on quadrate joint anatomy (joint) in mallards

Cross	Duck A skull	Duck A joint	Duck B skull	Duck B joint	Duck C skull	Duck C joint
N×Q_{rz}	0.96±0.03	0.98±0.01	0.95±0.02	0.97±0.01	0.82±0.08	0.96±0.01
N×Q_{ry}	–0.84±0.14	–0.66±0.03	–0.36±0.17	–0.86±0.03	NS	–0.44±0.10
N×Q_{rx}	0.66±0.15	0.70*	0.93±0.03	0.6±0.07	0.86±0.08	0.66±0.15
N×M	–0.76±0.23	–0.76±0.24	–0.80±0.08	–0.87±0.03	–0.47±0.32	–0.42±0.31
M×Q_{rz}	–0.88±0.12	–0.82±0.16	–0.89±0.03	–0.87±0.02	–0.76±0.14	0.17±0.8
M×Q_{ry}	0.89±0.04	0.93±0.01	0.62±0.09	0.88±0.04	0.65±0.11	0.82±0.02
M×Q_{rx}	0.84±0.04	0.77±0.12	–0.72±0.06	–0.2±0.18	–0.11±0.76	0.47±0.20

NS, not significant (neither of the N×Q_{ry} correlations were significant for Duck C in the skull JCS).
*Only one of the N×Q_{rx} correlations was significant for Duck A in the joint JCS, so this is not a mean.

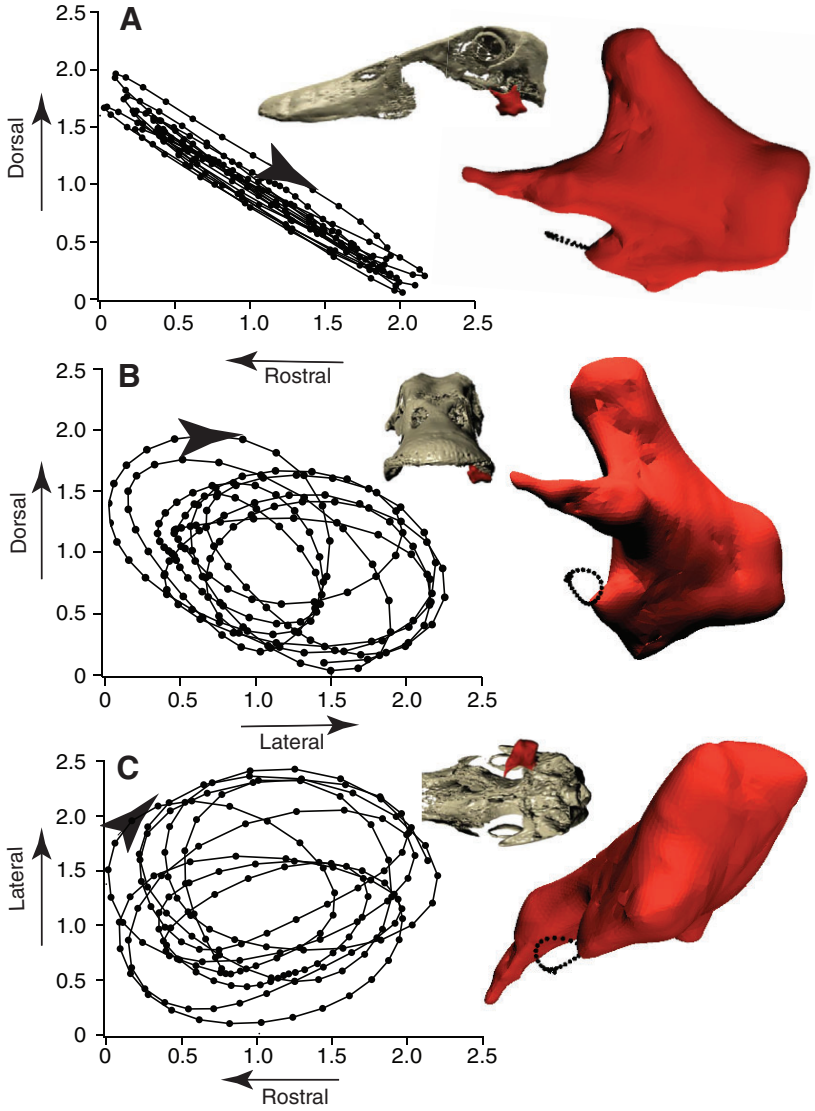

Fig. 10. The 3-D path of the pterygoid process of the left quadrate over nine feeding cycles (distances in mm). Corresponding images of the quadrate show the path over one cycle. (A) Lateral view. (B) Anterior view. (C) Ventral view. The path of pterygoid process is traced relative to the skull ACS. Each point on the graph represents 0.004 s. Arrows on the graphs show the direction of the movement as time increases.

quadrate could be the cause of the spreading of the mandibular rami rather than the result.

Quadrate kinematics

In agreement with previous studies, rostral rotation of the quadrate (positive Q_{rz}) is highly correlated with upper bill elevation (Figs 6, 8, 9). The JCS aligned with the planes of the skull defines an *X*-axis that runs through the body of the quadrate (Fig. 3C). Rotation about this *X*-axis is also closely correlated with upper bill elevation (Fig. 9). As the quadrate rotates rostrally about the *Z*-axis and the upper bill elevates, the quadrate rotates counterclockwise (left quadrate, when viewed from a ventral perspective) about the *X*-axis. The rostral and counterclockwise rotations could be caused by the action of the protractor quadrati muscle. This muscle originates on the basisphenoid, squamosal and interorbital septum of the skull and inserts on the orbital process of the quadrate and the mediodorsal and mediorostral aspects of the quadrate (Zweers, 1974). The protractor quadrati could rotate the quadrate inwards about the *X*-axis in addition to pulling it rostrally, corresponding to the counterclockwise rotation we observed during upper bill elevation. A more direct rostral pull could come from the pterygoid and its associated protractor muscle, the protractor pterygoidei.

Unexpectedly, the quadrate rotates laterally (positive Q_{ry}) during the latter half of upper bill elevation (Fig. 9A, Fig. 10). Previous studies of other species have suggested that if the quadrate does undergo a mediolateral rotation, then medial rotation should occur during jaw opening because the pterygoid is medial to the quadrate (Merz, 1963; Elzanowski, 1977; Gussekloo et al., 2001). There are no muscles inserting directly on the lateral surface of the quadrate, so the most probable cause of lateral quadrate rotation is lateral spreading of the mandibular rami transmitted through the quadrato-mandibular joint (although the possibility that lateral rotation of the quadrate is causing the observed mandibular bowing cannot be ruled out). The combination of rostromedial then rostrolateral motion causes the pterygoid process to trace an ellipse in ventral view (Fig. 10C).

The quadrate's interaction with the jugal may be important to understanding quadrate kinematics, but we were not able to measure jugal motion in this study. The jugal articulates with the lateral surface of the quadrate and could limit some of the rotations. It is also possible in mallards that the thin jugal is deforming.

Quadrate kinematics are complex, and choosing a functionally relevant JCS is therefore difficult. We chose a primary JCS based on the anatomical planes of the skull as it allows us to interpret the rotations of the quadrate strictly as movements in anatomical

directions (dorsal, lateral and rostral). We also tested a JCS aligned with the long axis of the quadrato-squamosal joint (Fig. 1) to see whether the motion of the quadrate could be described more simply, i.e. with fewer degrees of freedom. If this JCS provides a simpler description of the motion, then it should capture more of the quadrate motion as Q_{rz} than is captured by the Q_{rz} of our primary JCS, and Q_{ry} and Q_{rx} should be relatively smaller. For example, the nasofrontal joint is a hinge joint, so we expect rotation mainly about the *Z*-axis. Our nasofrontal JCS provides a good (i.e. simple) description of upper bill kinematics because almost all of the motion is captured in one variable, N_{rz} (Fig. 4). Compared with our primary JCS, we did not find that the JCS aligned with the quadrato-squamosal joint provided a simpler description of quadrate motion (Figs 6, 7, Table 4).

Mandibular bowing – diversity, cause and function

Intramandibular flexion (i.e. streptognathy) is known to occur in several groups of birds (e.g. Bühler, 1981; Zusi and Warheit, 1992; Zusi, 1993), but has not been evaluated in most kinematic analyses of cranial kinesis. Intramandibular flexion as an aid to prey capture and prey transport has been studied in several species including a pelican (Meyers and Myers, 2005; Burton, 1977), three hummingbirds (Yanega and Rubega, 2004), and an owl, nighthawks and swifts [see Bühler (Bühler, 1981) for references]. Zusi (Zusi, 1967) proposes that lateral spreading of the rami of the mandible disengages the locking mechanism between the quadrate and mandible and thus allows mandibular depression to be decoupled from upper bill elevation. Bühler (Bühler, 1981) suggests that intramandibular flexion may be present in anatids, based on data from other water-foraging birds, but streptognathy has not been previously demonstrated in mallards. Here we interpret movement of the rami in terms of quadrate–mandible interactions. Unfortunately, only one of the ducks we analyzed had markers in both rami, so we can only give qualitative evidence for the relationship between rami spreading and mandible depression.

The maximum intermandibular distance occurs during jaw opening (Fig. 5). The rami may spread because of the action of the depressor mandibulae muscle as it inserts laterally on the mandible. The lateral spreading of the mandible could in turn rotate the quadrate laterally as it swings rostrally during the second half of upper bill elevation. The mechanisms and function of streptognathy remain somewhat unclear in mallards, but are likely linked to quadrate movement and merit further investigation.

Coupled kinesis

We observed that upper and lower bill movements are correlated in the cycles that we analyzed (Fig. 9B), and that the upper bill elevates slightly (10 ms) ahead of mandibular depression (Fig. 9A). These results suggest some degree of coupled kinesis, but it is important to remember that our quadrato-mandibular JCS measures lower bill motion relative to the quadrate whereas upper bill motion is measured relative to the skull. Thus our comparisons of upper and lower motion differ somewhat from traditional measures of coupled kinesis. In addition, we deliberately selected sections of data to analyze that showed the most consistent sinusoidal motions of the upper and lower bills (in order to describe typical quadrate motion). In other sections of feeding trials, the relationship between upper and lower bill motion was more complex and variable (supplementary material Fig. S2), suggesting facultative rather than obligate coupling.

Nonetheless, we did find an interesting and consistent time lag between upper bill elevation at the nasofrontal joint and lower bill depression at the quadrato-mandibular joint during sinusoidal bill movements. This result is consistent with Zweers' (Zweers, 1974) electromyography data for mallard feeding showing the protractor quadrati to be active slightly before the jaw depressor muscles. Bout and Zeigler (Bout and Zeigler, 1994) observed in the pigeon that upper bill elevation occurs before mandibular depression, but protractor quadrati activation does not always precede depressor mandibulae activation. They proposed that the protractor quadrati muscle may 'unlock' the lower bill by moving the quadrate forward and upward, thus slacking the postorbital ligament. Zusi (Zusi, 1967) noted that species with large retroarticular processes, such as anatids, have correspondingly large depressor mandibulae muscles, which open both bills *via* the quadrato-mandibular articulation. This coordination of both bills through one muscle may be beneficial for small, repetitive and fast jaw movements, as occurs during filter feeding in mallards.

We cannot draw clear conclusions about the role of ligaments in coupled kinesis from this study as we did not manipulate the lacrymomandibular or postorbital ligaments. These ligaments may help regulate movements, but perhaps not as rigidly as previously described. Coupled kinesis through ligaments has been described through two-dimensional (2-D) force diagrams and four-bar models (Hoese and Westneat, 1996), but our results suggest that cranial kinesis in mallards is not a 2-D process, so these models may not apply. Future studies might include cutting the ligaments *in vivo* and measuring their effect on 3-D jaw kinematics as well as creating new 3-D models.

Concluding remarks

The mechanism of avian cranial kinesis involves the complex interaction of several skeletal elements. The quadrate, a central element, is not visible externally, so previous studies of quadrate kinematics have been limited to postmortem manipulations or mechanical models. Our *in vivo* XROMM results indicate that quadrate motion in mallards cannot be simplified to rotation about one primary axis, and the pterygoid process traces an elliptical pathway with substantial dorsoventral, mediolateral and rostrocaudal components (Fig. 10). It seems likely that quadrate movement is produced directly by the protractor quadrati muscle and indirectly by the depressor mandibulae through its articulation with the mandible.

We were not able to simplify quadrate motion by orienting a JCS to the morphology of the quadrato-squamosal joint. This result, combined with the complex motions of the quadrate, suggests that quadrate motion cannot be easily predicted from joint anatomy alone. The anatomy of the naso-frontal joint strongly suggests that it should act as a hinge joint, and indeed we found that motion at this joint can be described almost entirely by rotation about one axis. The anatomy of the quadrato-mandibular joint suggests that some sliding translations might be possible, but problems with our data because of mandibular bowing preclude testing this hypothesis.

Our conclusions for the mallard may not hold true for a passerine birds or even other anatids. Mallards have a large basipterygoid process, a large retroarticular process, a semi-functional joint between the dentary and supra-angular bones, and a deep, obliquely oriented medial articular cotyla. These features are not universally present in birds, so any effects they have on cranial kinematics may be unique to mallards. There are certainly differences in the degree to which important joints, such as the quadrato-squamosal and quadrato-mandibular joints, can move (Bühler, 1981). Comparative XROMM studies of species that share some of these anatomical

features with mallards would potentially allow us to make predictions about cranial kinematics from anatomy.

Future studies of avian cranial kinesis would benefit from *in vivo* methods as studies based only on postmortem manipulation may not reproduce the complex movements of the quadrate. Studies that link anatomical features to movement patterns and feeding behaviors may help further our understanding of avian skull evolution and phylogeny.

LIST OF ABBREVIATIONS

ACS	anatomical coordinate system
JCS	joint coordinate system
M	quadrato-mandibular joint
$M\times Q_{rx}$	mandibular *Z*-axis rotation cross-correlated with quadrate *X*-axis rotation
$M\times Q_{ry}$	mandibular *Z*-axis rotation cross-correlated with quadrate *Y*-axis rotation
$M\times Q_{rz}$	mandibular *Z*-axis rotation cross-correlated with quadrate *Z*-axis rotation
M_{rx}	rotation about the *X*-axis of the quadrato-mandibular joint
M_{ry}	rotation about the *Y*-axis of the quadrato-mandibular joint
M_{rz}	rotation about the *Z*-axis of the quadrato-mandibular joint
N	nasofrontal joint
N×M	nasofrontal *Z*-axis rotation cross-correlated with mandibular *Z*-axis rotation
$N\times Q_{rx}$	nasofrontal *Z*-axis rotation cross-correlated with quadrate *X*-axis rotation
$N\times Q_{ry}$	nasofrontal *Z*-axis rotation cross-correlated with quadrate *Y*-axis rotation
$N\times Q_{rz}$	nasofrontal *Z*-axis rotation cross-correlated with quadrate *Z*-axis rotation
N_{rx}	rotation about the *X*-axis of the nasofrontal joint
N_{ry}	rotation about the *Y*-axis of the nasofrontal joint
N_{rz}	rotation about the *Z*-axis of the nasofrontal joint
N_{tx}	translation about the *X*-axis of the nasofrontal joint
N_{ty}	translation about the *Y*-axis of the nasofrontal joint
N_{tz}	translation about the *Z*-axis of the nasofrontal joint
Q	quadrato-squamosal joint
Q_{rx}	rotation about the *X*-axis of the quadrato-squamosal joint
Q_{ry}	rotation about the *Y*-axis of the quadrato-squamosal joint
Q_{rz}	rotation about the *Z*-axis of the quadrato-squamosal joint
SVD	singular value decomposition
XROMM	X-ray reconstruction of moving morphology

ACKNOWLEDGEMENTS

We thank the Brown University Morphology Group for reading and discussing the manuscript, and S. Gatesy for additional insightful suggestions. This project was funded by the W. M. Keck Foundation, the Bushnell Faculty Research Fund and the US National Science Foundation under grant numbers 0552051 and 0840950.

REFERENCES

Bishop, K. L. (2006). The relationship between 3-D kinematics and gliding performance in the southern flying squirrel, *Glaucomys volans*. *J. Exp. Biol.* **209**, 689-701.

Bock, W. J. (1964). Kinetics of the avian skull. *J. Morphol.* **114**, 1-42.

Bout, R. and Zeigler, H. P. (1994). Jaw muscle (EMG) activity and amplitude scaling of jaw movements during eating in pigeon (*Columba livia*). *J. Comp. Physiol. A* **174**, 433-442.

Bout, R. G. and Zweers, G. A. (2001). The role of cranial kinesis in birds. *Comp. Biochem. Physiol.* **131A**, 197-205.

Brainerd, E. L., Baier, D. B., Gatesy, S. M., Hedrick, T. L., Metzger, K. A., Gilbert, S. L. and Crisco, J. J. (2010). X-ray reconstruction of moving morphology (XROMM): precision, accuracy and applications in comparative biomechanics research. *J. Exp Zool.* **313A**, 262-279.

Bühler, P. (1981). Functional anatomy of the avian jaw apparatus. In *Form and Function in Birds* (ed. A. S. King and J. McLellard), pp. 439-468. New York: Academic Press.

Burton, P. J. K. (1977). Lower jaw action during prey capture by pelicans. *Auk* **94**, 785-786.

Cracraft, J. (1986). The origin and early diversification of birds. *Paleobiology* **12**, 383-399.

Elzanowski, A. (1977). On the role of basipterygoid processes in some birds. *Verh. Anat. Ges.* **71**, 1303-1307.

Elzanowski, A., Paul, G. S. and Stidham, T. A. (2000). An avian quadrate from the Late Cretaceous Lance Formation of Wyoming. *J. Vertebr. Paleontol.* **20**, 712-719.

Estrella, S. M. and Masero, J. A. (2007). The use of distal rhynchokinesis by birds feeding in water. *J. Exp. Biol.* **210**, 3757-3762.

Gatesy, S. M., Baier, D. B., Jenkins, F. A. and Dial, K. P. (2010). Scientific rotoscoping: a morphology-based method of 3-D motion analysis and visualization. *J. Exp. Zool.* **313A**, 244-261.

Goodman, D. C. and Fisher, H. I. (1962). *Functional Anatomy of the Feeding Apparatus in Water Fowl (Aves: Anatidae)*. Carbondale: Southern Illinois University Press.

Green, J. R., Moore, C. A., Higashikawa, M. and Steeve, R. W. (2000). The physiologic development of speech motor control: lip and jaw coordination. *J. Speech Lang. Hear. Res.* **43**, 239-255.

Gurd, D. B. (2006). Filter-feeding dabbling ducks (*Anas* spp.) can actively select particles by size. *Zoology* **109**, 120-126.

Gurd, D. B. (2007). Predicting resource partitioning and community organization of filter-feeding dabbling ducks from functional morphology. *Am. Nat.* **169**, 334-343.

Gussekloo, S. W. S. and Bout, R. G. (2005). Cranial kinesis in palaeognathous birds. *J. Exp. Biol.* **208**, 3409-3419.

Gussekloo, S. W. S., Vosselman, M. G. and Bout, R. G. (2001). Three-dimensional kinematics of skeletal elements in avian prokinetic and rhynchokinetic skulls determined by Roentgen stereophotogrammetry. *J. Exp. Biol.* **204**, 1735-1744.

Hérissant, M. (1748). Observations anatomiques sur les mouvemens du bec des oiseaux. *Hist. Acad. R. Sci.* **1748**, 345-386.

Hoese, W. J. and Westneat, M. W. (1996). Biomechanics of cranial kinesis in birds: testing linkage models in the white-throated sparrow (*Zonotrichia albicollis*). *J. Morphol.* **227**, 305-320.

Merz, R. (1963). Jaw musculature of the morning and white-winged doves. *Univ. Kans. Publ. Mus. Nat. Hist.* **12**, 523-551.

Meyers, R. A. and Myers, R. P. (2005). Mandibular bowing and mineralization in brown pelicans. *Condor* **107**, 445-449.

Moore, C. A. (1993). Symmetry of mandibular muscle activity as an index of coordinative strategy. *J. Speech Hear. Res.* **36**, 1145-1157.

Nuijens, F. W., Hoek, A. C. and Bout, R. G. (2000). The role of the postorbital ligament in the zebra finch (*Taeniopygia guttata*). *Neth. J. Zool.* **50**, 78-88.

Rodgers, J. L. and Nicewander, W. A. (1988). Thirteen ways to look at the correlation coefficient. *Am. Stat.* **42**, 59-66.

Shao, X. M. and Tsau, Y. (1996). Measure and statistical test for cross-correlation between paired neuronal spike trains with small sample size. *J. Neurosci. Methods* **70**, 141-152.

Simonetta, A. M. (1960). On the mechanical implications of the avian skull and their bearing on the evolution and classification of birds. *Q. Rev. Biol.* **35**, 206-220.

Söderkvist, R. and Wedin, P. (1993). Determining the movements of the skeleton using well-configured markers. *J. Biomech.* **26**, 1473-1477.

Yanega, G. and Rubega, M. A. (2004). Hummingbird jaw bends to aid insect capture. *Nature* **428**, 615.

Tashman, S. and Anderst, W. (2003). In vivo measurement of dynamic joint motion using high-speed radiography and CT: application to canine ACL deficiency. *J. Biomech. Eng.* **125**, 238-245.

van Gennip, E. M. S. J. and Berkhoudt, H. (1992). Skull mechanics in the pigeon, *Columba livia*. A three-dimensional kinematic model. *J. Morphol.* **213**, 197-224.

Wren, T. A. L., Do, K. P., Rethlefsen, S. A. and Healy, B. (2006). Cross-correlation as a method for comparing dynamic electromyography signals during gait. *J. Biomech.* **36**, 2714-2718.

Zatsiorsky, V. M. (1998). *Kinematics of Human Motion*. Champaign, IL: Human Kinetics.

Zusi, R. L. (1967). The role of the depressor mandibulae muscle in kinesis of the avian skull. *Proc. U. S. Nat. Mus. Smith. Inst.* **123**, 1-23.

Zusi, R. L. (1984). A functional and evolutionary analysis of rhynchokinesis in birds. *Smith. Contr. Zool.* **395**, 1-40.

Zusi, R. L. (1993). Patterns and diversity in the avian skull. In *The Skull*, Vol. 2 (ed. J. Hanken and B. A. Hall), pp. 391-437. Chicago IL: Chicago University Press.

Zusi, R. L. and Warheit, K. I. (1992). On the evolution of the intramandibular joints of pseudodontorns (Aves: Odontopterygia). In *Papers in Avian Paleontology Honoring Pierce Brodkorb. Natural History Museum of Los Angeles County, Science Series No. 36* (ed. K. E. Campbell, Jr), pp. 351-360. Los Angeles, CA: Natural History Museum of Los Angeles County.

Zweers, G. A. (1974). Structure, movement and myography of the feeding apparatus of the Mallard (*Anas platyrhynchos* L.) a study in functional anatomy. *Neth. J. Zool.* **24**, 323-467.